TECHNICAL MEMORANDUM

743

# The evolution of the ECMWF hybrid data assimilation system

Massimo Bonavita, Elias Holm,
Lars Isaksen and Mike Fisher

Research Department

December 2014

To be submitted for publication in Quart. J. Roy. Meteor. Soc



European Centre for Medium-Range Weather Forecasts
Europäisches Zentrum für mittelfristige Wettervorhersage
Centre européen pour les prévisions météorologiques à moyen

Series: ECMWF Technical Memoranda

A full list of ECMWF Publications can be found on our web site under:
http://www.ecmwf.int/en/research/publications

Contact: library@ecmwf.int



European Centre for Medium Range Weather Forecasts
Shinfield Park, Reading, Berkshire RG2 9AX, England

**Abstract**

The trend towards using flow-dependent, ensemble-based estimates of background error covariances has been one of the main themes of atmospheric data assimilation research and development in recent years. In this work it is documented how flow-dependent ensemble information from the ECMWF EDA has gradually been incorporated into the B model which describes the background error covariance matrix at the start of the ECMWF 4DVar assimilation window. Starting with background error variances for the balanced part of the control vector and observation quality control (Bonavita et al., 2012) the current paper extends the flow-dependency to background error variances for the unbalanced part of the control vector and for background error correlation structures. The correlations are determined either online from previous days or from a hybrid of climatological and current cycle estimates. Each of these changes is shown to improve both the realism of the modelled B and the accuracy of the analysis and forecast fields produced by the 4DVar assimilation cycle which makes use of the improved B. Finally, increasing the resolution at which the EDA 4DVars are run is shown to reduce the under-dispersiveness of the EDA-based error estimates.

# 1 Introduction

A main trend in the development of data assimilation schemes in recent years is the effort towards more accurate and flow-dependent estimates of background error covariances. Variational methods used in operational data assimilation systems are moving from static, climatological representation of the background error covariance matrix **B** (Fisher, 2003, Belo Pereira and Berre, 2006) to ensemble-based, flow-dependent **B** matrix models (Buehner et al. 2010a, b; Bishop and Hodyss 2011; Clayton et al. 2012; Wang et al., 2013). These hybrid assimilation systems usually combine the static **B** model used in standard variational data assimilation with a flow-dependent estimate of **B** which is directly sampled from the ensemble and is further regularized through spatial localization ("alpha control variable" method, Barker, 1999, Hamill and Snyder, 2000, Lorenc, 2003, Buehner, 2005). This methodology can be extended to use sampled estimates of the background error covariance matrix throughout the length of the window (4D-En-Var, Liu et al., 2008). Another approach is the ensemble Kalman filter (EnKF, Evensen, 1994, Burgers et al., 1998) which directly samples ensemble short range forecasts to provide low-dimensional flow-dependent representation of the background error covariances. Finally, short range ensemble forecasts can provide flow-dependent input to a parametric **B** model, as in the ECMWF Ensemble of Data Assimilations (EDA, Isaksen et al. 2010) system.

The EDA represents the evolution of the high resolution (HRES) 4DVar assimilation errors through an ensemble of lower resolution 4DVar analysis cycles which make use of perturbed observations, perturbed sea surface temperature (SST) fields and perturbed model physical tendencies. The short range forecasts from the EDA are used to calibrate the wavelet background model used in the standard ECMWF 4DVar (Fisher, 2003), which provides flow-dependent information in the modelled **B**. The ECMWF wavelet **B** model can be formally represented as a sequence of linear operators (Fisher, 2003):

$$\mathbf{B} = \mathbf{T}^{-1}\boldsymbol{\Sigma}_b^{1/2}\mathbf{C}\boldsymbol{\Sigma}_b^{1/2}\mathbf{T}^{-T} \tag{1}$$

where **T** is a matrix representation of the balance operator (i.e., the operator that maps the control vector used in the variational analysis to the model variables), $\boldsymbol{\Sigma}_b^{1/2}$ is the diagonal matrix of background error

standard deviations and **C** is the background error correlation operator (which is modelled in wavelet space). The ECMWF 4DVar analysis, in common with other variational analysis systems, is computed in a different space than that defined by the set of atmospheric model variables, which in the ECMWF Integrated Forecast System (IFS) are vorticity, divergence, temperature, logarithm of surface pressure, specific humidity and ozone [ζ, η, (T, ln($p_s$)), q, $O_3$]. The aim is to construct a set of variables (the "control vector") which are approximately uncorrelated, so that the corresponding **B** matrix can be simplified to a block diagonal formulation in spectral or wavelet space. In the ECMWF implementation (Derber and Bouttier, 1999), the control vector is composed by the standard variables [ζ, q, $O_3$] plus the "unbalanced" components of divergence, temperature and logarithm of surface pressure, [$\eta_u$, (T, ln($p_s$))$_u$]. The multivariate correlations between the model variables are then implicitly represented through the specific functional forms chosen for the balance operator (i.e., the **T** term in Eq. (1)). In previous work (Bonavita et al., 2012) the beneficial impact on the ECMWF analysis of using a spatially filtered estimate of background error standard deviations ($\mathbf{\Sigma}_b^{1/2}$) from the EDA was demonstrated for the standard part of the control vector ([ζ, q, $O_3$]) plus a set of other variables that are used in the observations quality control algorithm (i.e., temperature, wind components, relative humidity and geopotential). Section 2 of this paper presents the impact on the performance of the ECMWF analysis system of extending the use of EDA perturbations to estimate the unbalanced part of the control vector. This follows the work of Raynaud et al., 2011, where the impact of unbalanced EDA errors was evaluated in Météo-France global 4DVar system. Section 3 evaluates the impact of using the EDA perturbations to perform an online calibration of the correlation structures of the **B** matrix (i.e., the **C** term in Eq. (1)).

The computational cost of running an ensemble of independent 4DVar cycles in the EDA makes it necessary to reduce the size of the ensemble and the spatial resolution of its members that can conveniently be run in the operational schedule. The sampling errors introduced in the estimation of **B** by the limited ensemble size, and methods to control them, have been extensively discussed for background error standard deviations (Berre et al., 2007; Raynaud et al., 2008, 2009; Bonavita et al., 2011; Raynaud et al., 2012; Pannekoucke et al., 2014) and for the background error correlation structures (Pannekoucke et al., 2007; Pannekoucke et al., 2008; Varella et al., 2011). An aspect that has received less attention is the impact of the different, considerably smaller resolution at which the EDA members are currently run with respect to the resolution of the target assimilation system whose error statistics they are used to simulate. The sensitivity of the EDA-derived error estimates to the resolution at which the EDA 4DVars are run is examined and some preliminary results are described in Section 4.

The development strategy described in this paper follows the general idea of using perturbations from an ensemble data assimilation system to construct online estimates of a parametric **B** model. Relative strengths and limitations of this approach are discussed in Section 5. A summary of the main findings is provided in Section 6.

## 2 EDA Variances for the unbalanced control vector

EDA-based estimation of the background error variances of the day for the standard variables [ζ, q, $O_3$] was implemented in the ECMWF Integrated Forecasting System (IFS) in Cycle 37R2 (May 2011), as described in Bonavita et al. (2012). This formulation projects flow-dependent information from the EDA error estimates of vorticity into the error estimates for the balanced components of divergence, temperature and surface pressure ([η, (T,$p_s$)]) through the balance operators, while leaving the

background error variance of the unbalanced components ($[\eta_u, (T,ps)_u]$) static. The balance operators themselves are also flow-dependent because they are based on versions of the non-linear balance and omega equations linearized around the background state (Fisher, 2003). However, as shown in Fig. 1, the error variance of the unbalanced components ($[\eta_u, (T,p_s)_u]$) contributes significantly to the total error variance of these variables. This figure can be qualitatively compared with the bottom panel of Fig. 10 in Bouttier et al. (1997). It is apparent how the fraction of the temperature errors that can be explained by the balance constraints has considerably reduced in the troposphere since 1996. This is interpreted as a consequence of the much more accurate estimates of the atmospheric initial conditions the data assimilation system currently produces, which lead to a reduction in both the magnitude and the spatial scale of the analysis increments in successive assimilation cycles. It is thus potentially important to move from a spatially homogeneous, static estimate of the errors of the unbalanced part of the 4DVar control vector to an EDA-based, flow-dependent one. This upgrade has been implemented at ECMWF in IFS cycle 38R2 (June 2013). An example of the structure of the diagnosed errors is presented in Fig. 2, where the zonally and monthly time averaged vertical profiles of the unbalanced component of temperature (left panel) and divergence (right panel) are shown, and in Fig. 3, where the monthly average of the errors of unbalanced pressure are shown. Unbalanced errors tend to be relatively larger in the Tropics and around low pressure systems in the Extra-Tropics for surface pressure. In the vertical unbalanced errors have maxima in the upper troposphere lower stratosphere (UTLS) around model level 60 (ca. 100 hPa), in a layer near the stratopause (model levels 10 to 20, ca. 1-3 hPa), and in the planetary boundary layer (model levels 115 to 137, ca. 850 hPa to surface). These are the regions where the mass-wind balance built in the 4DVar is least effective in explaining the errors for the total variables.

The effect of including flow-dependency in the unbalanced errors on the high resolution data assimilation (T1279 outer loop, T159/T255/T255 inner loops) was investigated by running experiments with flow-dependent versus static unbalanced errors using the pre-operational version of IFS Cycle 38R2. Figure 4 shows the standard deviation of the difference of the analysis increments of these assimilation experiments over a period of a month for temperature (left panel), and the meridional component of wind (right panel), while Fig. 5 shows a geographical plot of the same diagnostic computed for the surface pressure. A clear correlation between these last plots and the corresponding unbalanced errors shown in Figs. 2-3 can be seen.

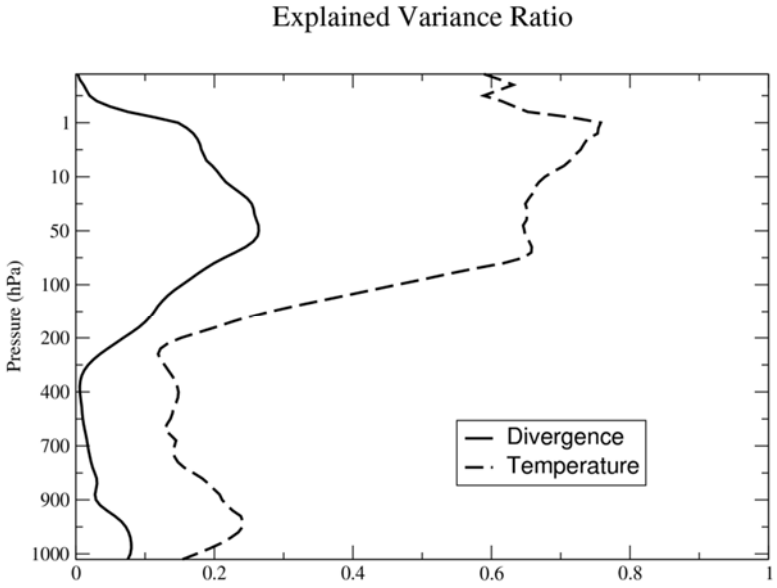


*Figure 1: Vertical profiles of the fraction of the total background error variance of divergence (continuous line) and temperature (dashed line) that is explained by the balance relationship with the vorticity errors.*

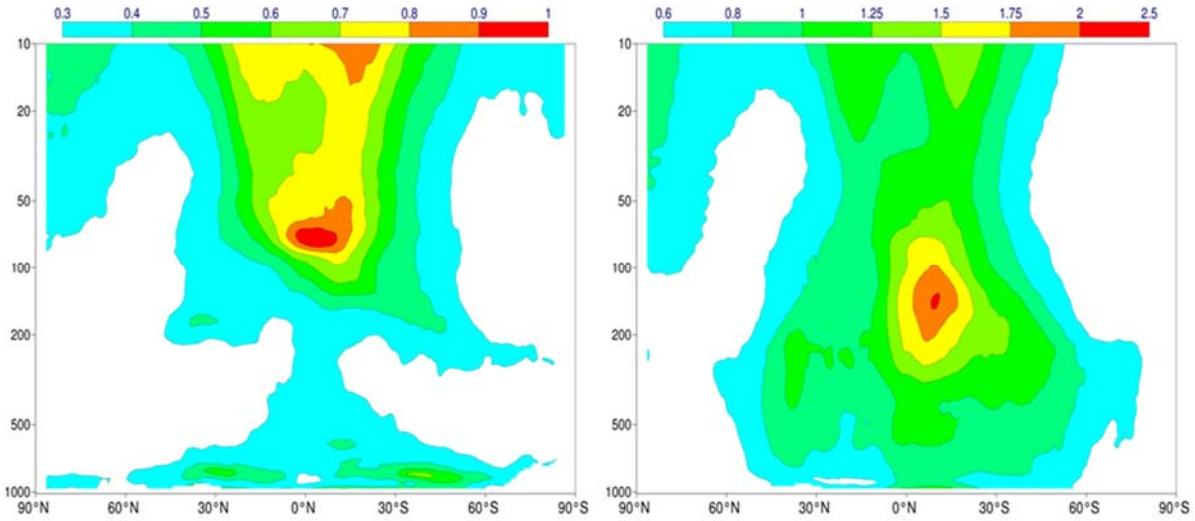


*Figure 2: Vertical profiles of the longitudinally averaged EDA standard deviations of unbalanced temperature (left panel) and unbalanced divergence (right panel). Values are time averaged over one month (March 2012).Units in Kelvin (temperature) and $10^{-5}$ $s^{-1}$ (divergence). Vertical axis in pressure (hPa).*

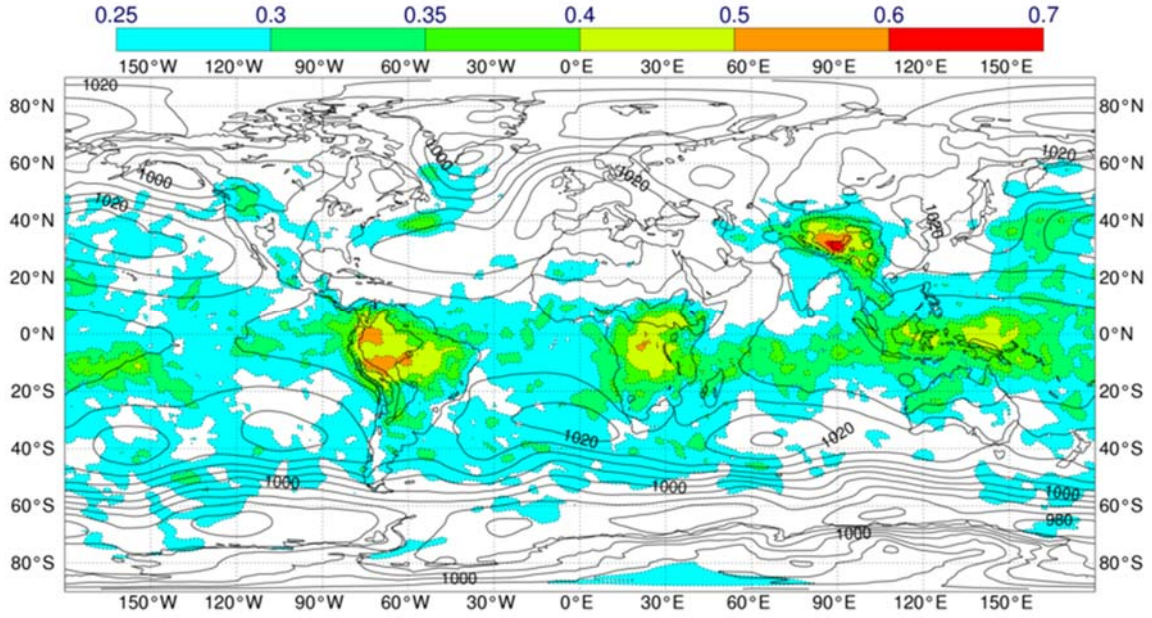


*Figure 3: Time averaged (March 2012) EDA standard deviation of the unbalanced component of the surface pressure (shaded; hPa) and Mean Sea level pressure from ECMWF operational analysis (black contours; hPa).*

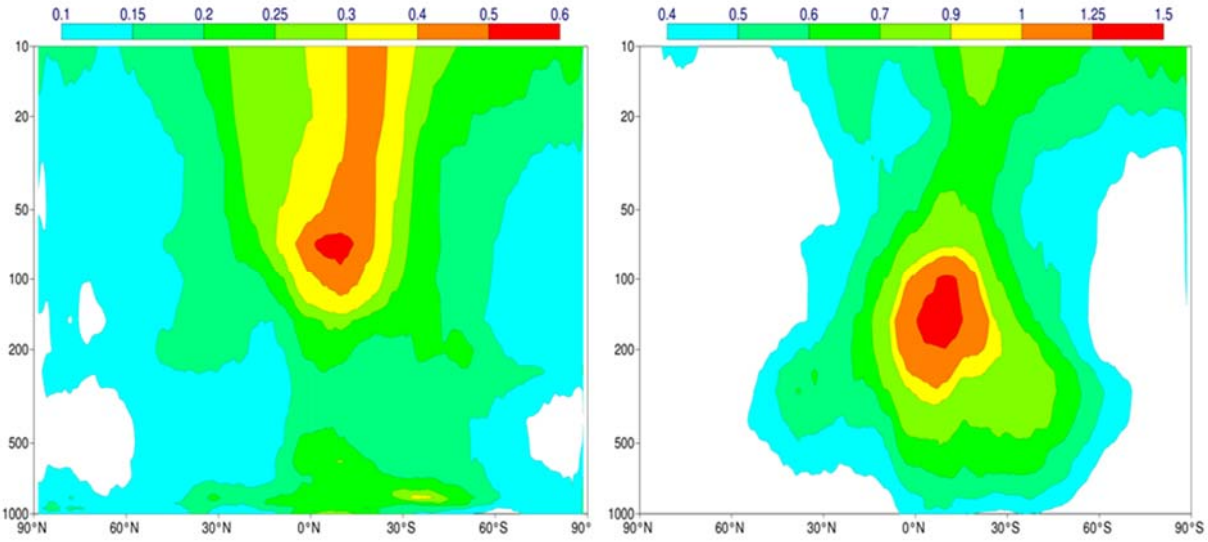


*Figure 4: Vertical profiles of the longitudinally averaged standard deviation of the difference between the temperature (left panel) and meridional wind (right panel) analysis increments of the assimilation experiments using/not using the EDA estimates of the errors of the unbalanced control vector. Values are time averaged over 1 month (March 2012).Units in Kelvin (temperature) and m/s (v wind). Vertical axis is labelled in pressure levels (hPa).*

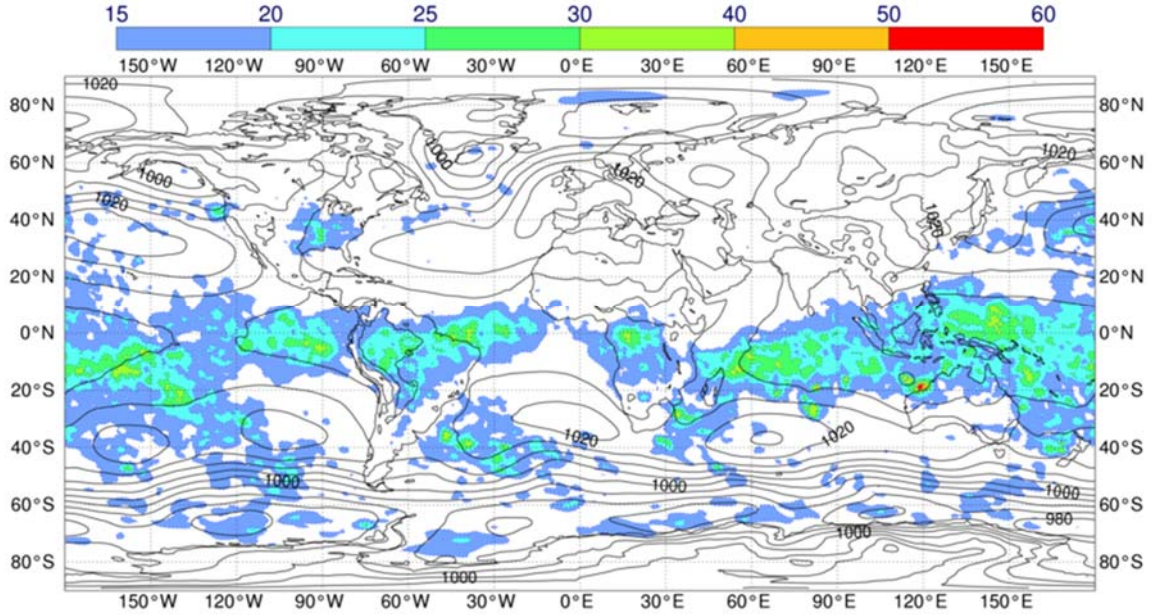


*Figure 5: Standard deviation of the difference between the surface pressure analysis increments of the assimilation experiments using/not using the EDA estimates of the errors of the unbalanced control vector (shaded; hPa) and Mean Sea level pressure from ECMWF operational analysis (black contours; hPa).*

Having verified that the introduction of spatial structures in the unbalanced control vector errors introduces correspondingly structured increments in the 4DVar analysis, the next question is to investigate how these increments affect the analysis and forecast accuracies.

In terms of analysis skill, it is useful to consider the change in analysis and background departures for GPS based radio occultation measurements (GPSRO) as these observations have global spatial distribution and sufficient vertical resolution from the upper troposphere to middle stratosphere (Bonavita, 2014 and references therein). With flow-dependent unbalanced errors the analysis fits observations closer in the tropical stratosphere and less so in the extra-tropical stratosphere (Fig.6, left column). This is a consequence of the fact that the globally averaged background error standard deviations are by design prescribed from the covariance matrix used in the ECMWF 4DVar so that an increase of errors in the Tropics then leads to decrease in the Extra-Tropics. This also implies that a smaller fraction of the total temperature and wind error is apportioned to the balanced modes in the Tropics while a larger fraction is in the Extra-Tropics, so the extra-tropical analysis increments become more geostrophic. In terms of changes to the background departure standard deviations (Fig. 6, right column), the impact of EDA-based unbalanced control vector errors is seen to be neutral in the Tropics but positive in the Extra-Tropics.

The impact of EDA-based unbalanced control vector errors on the assimilation cycle described above carries over in a rather consistent way on the forecast behaviour of the two experiments. This is shown in Fig. 7 for the root mean square error of geopotential forecasts, and displays a nearly homogeneous improvement throughout the atmospheric column and the different regions of the globe. The apparent degradation in the first two days of forecast in the tropical stratosphere is likely due to the increased variability of the analysis using the EDA-based unbalanced control vector errors, as no degradation is apparent in the verification against radiosondes (not shown).

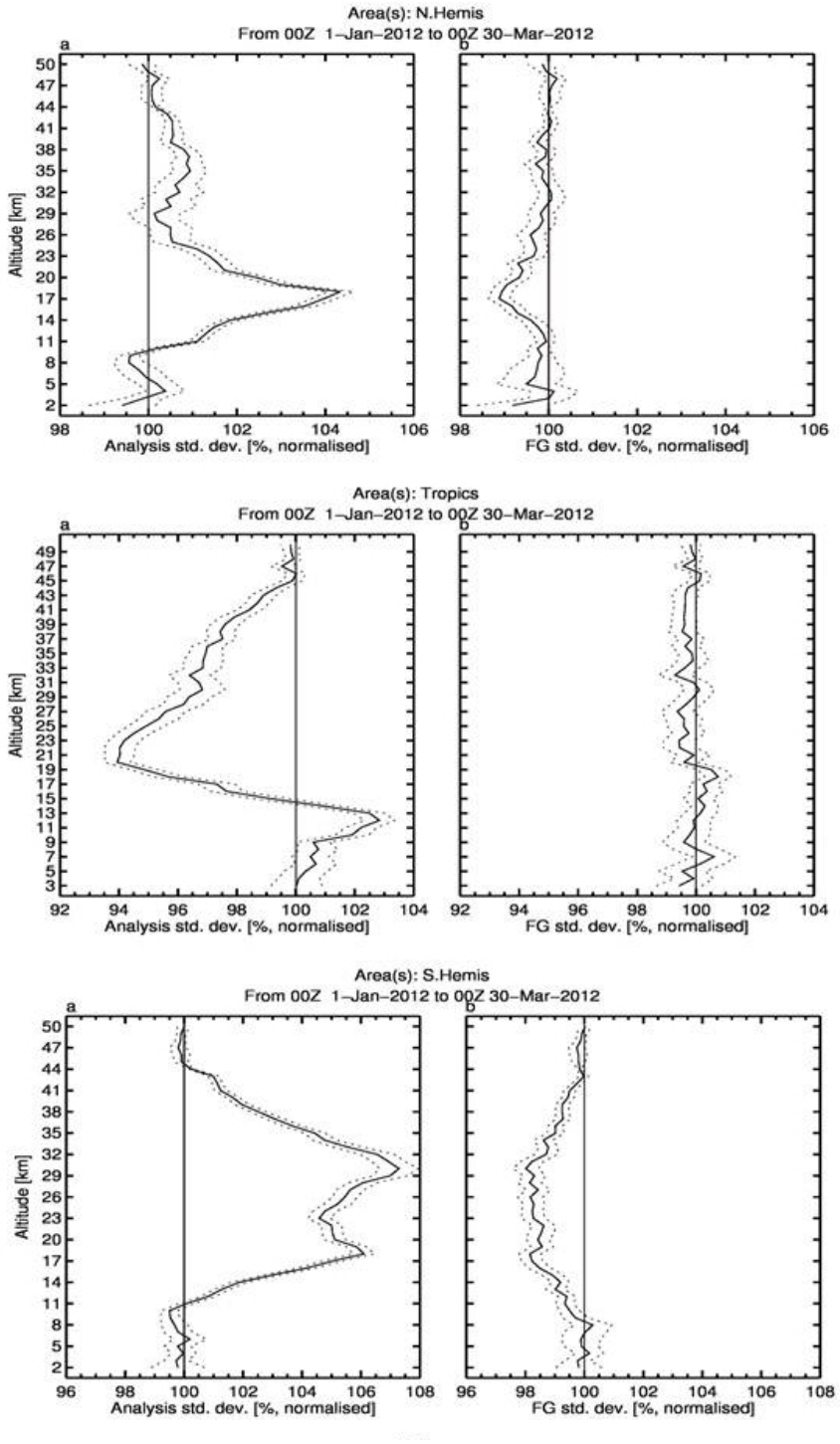


*Figure 6: Normalised change in the standard deviation of analysis departures (left column) and background departures (right column) of assimilated GPSRO observations for experiments using/not using the EDA-based estimates of unbalanced control vector errors. First row: Northern Hemisphere; second row: Tropics; third row: Southern Hemisphere. Values averaged over the 1/1/2012 - 30/3/2012 period. Dotted lines represent 95% confidence intervals.*

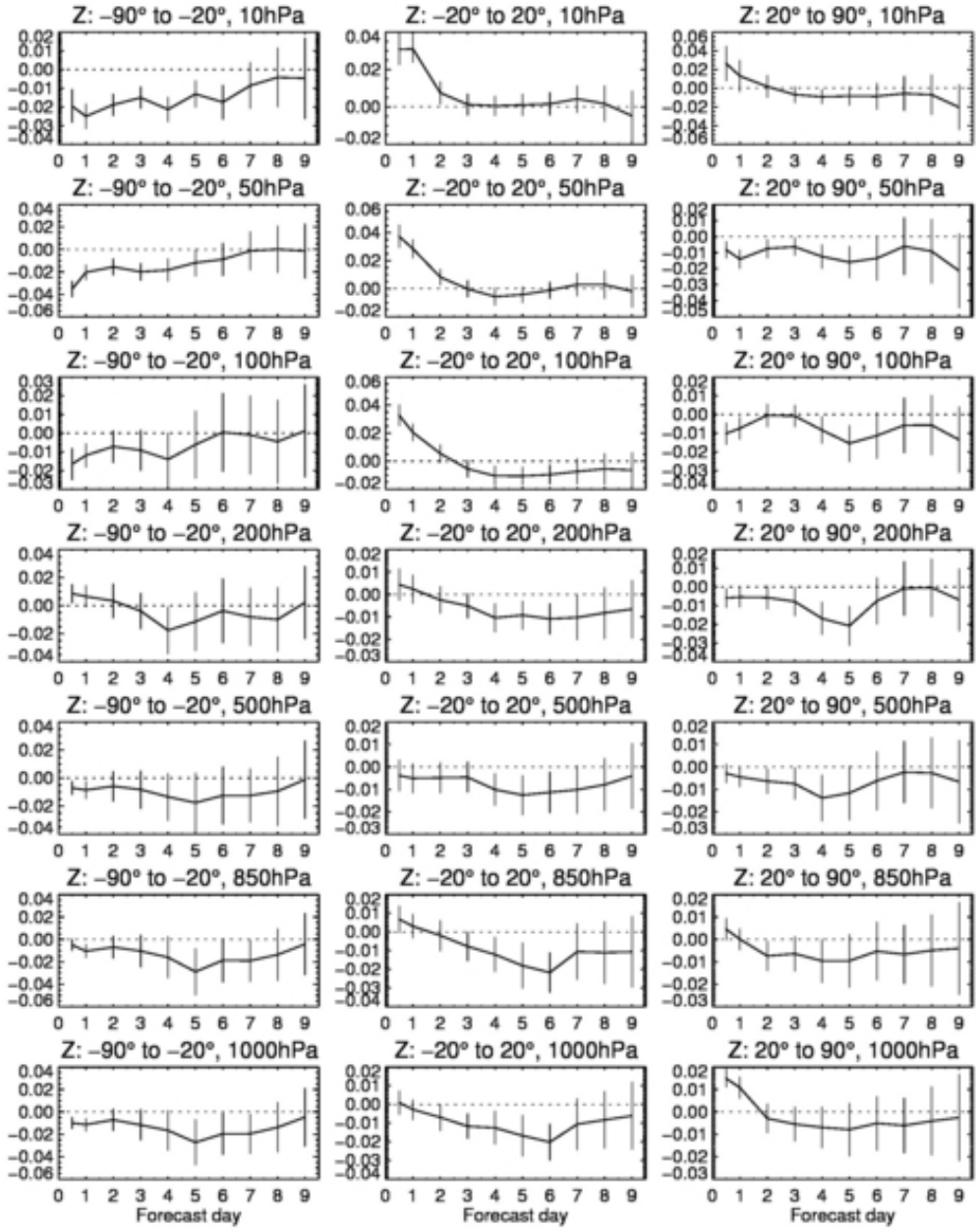


*Figure 7: Normalised difference in RMSE of geopotential forecasts for the assimilation experiments using/not using EDA-based unbalanced control vector errors (negative values imply smaller errors for the experiment using EDA-based error estimates). First column refers to the Southern Hemisphere; second column to the Tropics; third column to the Northern Hemisphere. Scores are averaged over the period 01/01/2012 - 30/03/2012 and computed using own analysis as verification. Dotted lines represent 95% confidence intervals.*

# 3 Online estimation of error correlation structures

The wavelet formulation of the background error correlation structure functions (term **C** in Eq. 1) introduced by Fisher, 2003, allows the ECMWF **B** model to represent both scale-dependent (i.e., spectral) and location dependent (spatial) heterogeneities of the underlying correlation field. However its computation has been based on a climatological sample of EDA perturbations. The non-negligible

temporal and flow-dependent dynamics of the error correlations (Varella et al., 2011) imply that an online calibration of wavelet **B** model should be able to provide a more accurate description of the underlying correlation structures, especially in areas characterized by the presence of active weather systems. In practice, it has been found that a calibration dataset of around 500 to 600 perturbation samples is necessary to get robust estimates for the wavelet **B** model with a suitably low noise level, with no spatial localization or filtering applied either to the input perturbations or the ensuing sampled **B**. This obviously requires an EDA system whose size is considerably larger than what is currently, and in the near future, affordable to run (note that starting with IFS cycle 40R1, November 2013, the size of the EDA has been upgraded from 10 to 25 members). In order to adequately populate the training dataset of EDA perturbations, two solutions have been explored at ECMWF and will be described in the following: an online **B** estimate through lagged EDA background forecasts and a hybrid (online + climatological) **B** estimate.

a) Online wavelet B with lagged EDA perturbations.

One way of building a sufficiently large dataset of EDA perturbations is to use a 12 day sliding window of the latest EDA background forecasts. This form of regularizing the **B** estimates through time averaging obviously reduces the "flow-dependent" character of the diagnosed correlations, so that weather systems with large variability on time scales of a day or less (i.e., frontal systems, tropical cyclones, etc.) cannot be properly represented. On the other hand, errors connected to more stationary weather features (i.e., blocked flow regimes or slow moving centres of action) can be adequately described by the system.

Figure 8 shows the diagnosed background error length scales for vorticity at model level 96 (ca. 500 hPa) for the static wavelet **B** (top panel) and the online wavelet **B** (bottom panel). While the static wavelet **B,** which is computed from a composite of summer/winter samples, captures the spatial distribution of the "climatological" weather patterns in the area and the distribution of the observing system, the online wavelet **B** is able to add structures that are relevant to the prevailing flow regime, i.e. correlation length scales tend to become shorter in low pressure areas and larger in high pressure regions. This response of the online wavelet **B** to the locally prevailing weather pattern is also visible in the vertical correlation structures. In this regard, consider the three meteorological situations depicted in Figs. 9-10 in the North-eastern Pacific. For the location highlighted with an arrow at (30N, 140W), the prevailing weather pattern is characterized by the presence of an extensive stratocumulus layer (Fig. 9, top panel), an high pressure configuration (Fig. 10, top panel right) and a sharp temperature inversion below 850 hPa (Fig. 10, top panel left). This predominant weather pattern is reflected in the vertical profile of background error correlations diagnosed from the climatological wavelet **B**. The vertical correlation of vorticity centred at model level 115 (ca. 850 hPa; Fig. 11, black continuous line) is sharp and, in the boundary layer, decreases rapidly to less than 0.1 at levels below 925 hPa (model level 122). In the middle panels of Figs. 9-10 (10 January 2012) the cyclonic flow has shifted equatorward and (30N, 140W) is marginally affected by frontal passages, the temperature inversion at the top of the marine boundary layer has weakened (Fig. 10, middle panel right) and the vertical error correlation has consistently broadened (Fig. 11, red continuous line). This effect is more pronounced in the meteorological situation depicted in the bottom panels of Figs. 9-10 (10 February 2012). The storm track has moved further south and (30N, 140W) is affected by a series of frontal passages. The result of this changed synoptic situation is a deeper, well mixed boundary layer (Fig. 10, bottom panel right) and a considerably broader vertical error correlation structure (Fig. 11, dashed line).

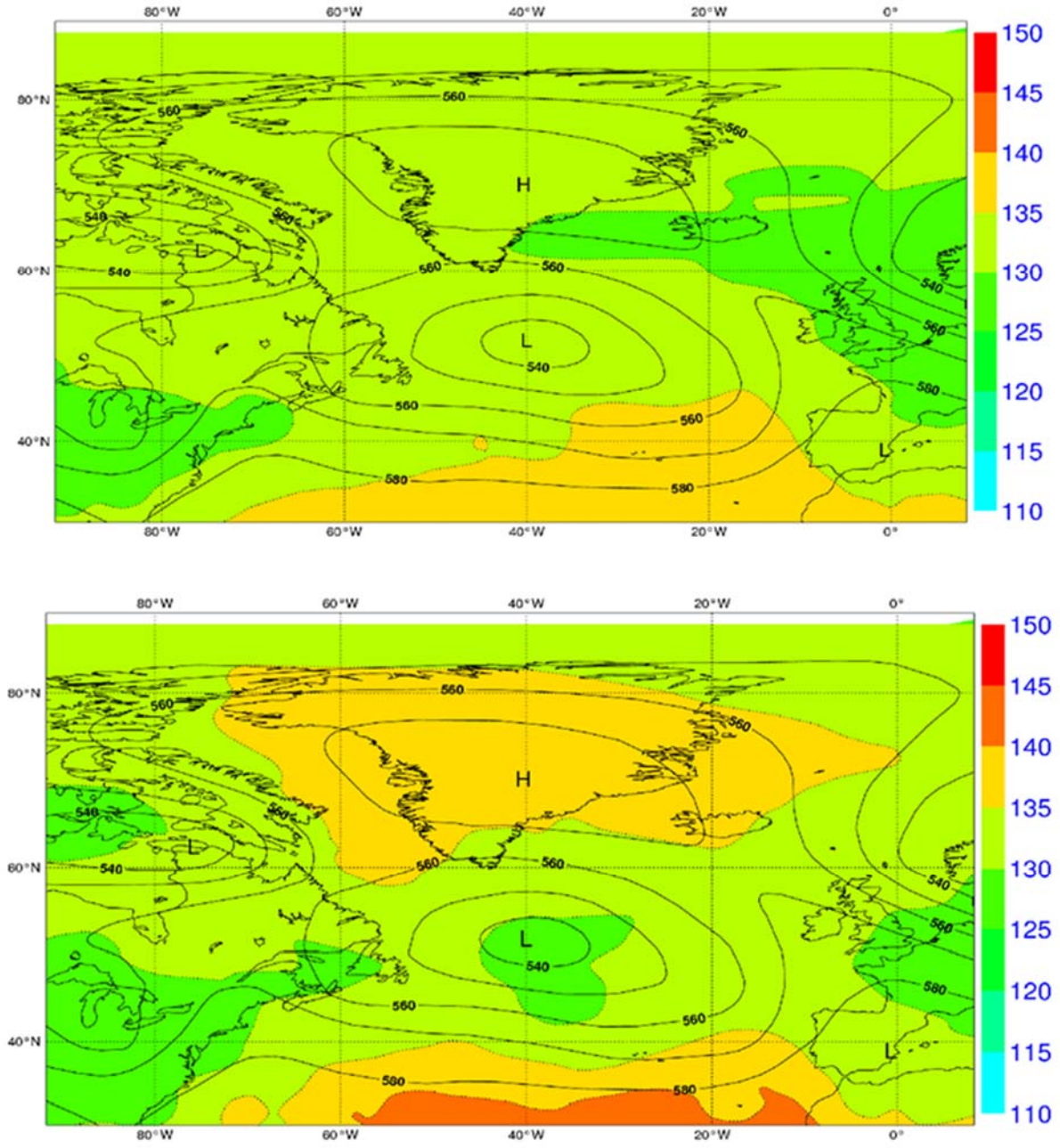


*Figure 8: Background error length scales (shaded; units: km)) for vorticity at model level 96 (~500 hPa) diagnosed from the static wavelet B (top panel) and the online wavelet B (bottom panel), valid on 01/06/2012 at 21UTC, and background 500 hPa geopotential pressure forecast valid at the same time (solid line, units: $10^2$ $m^2/s^2$)*

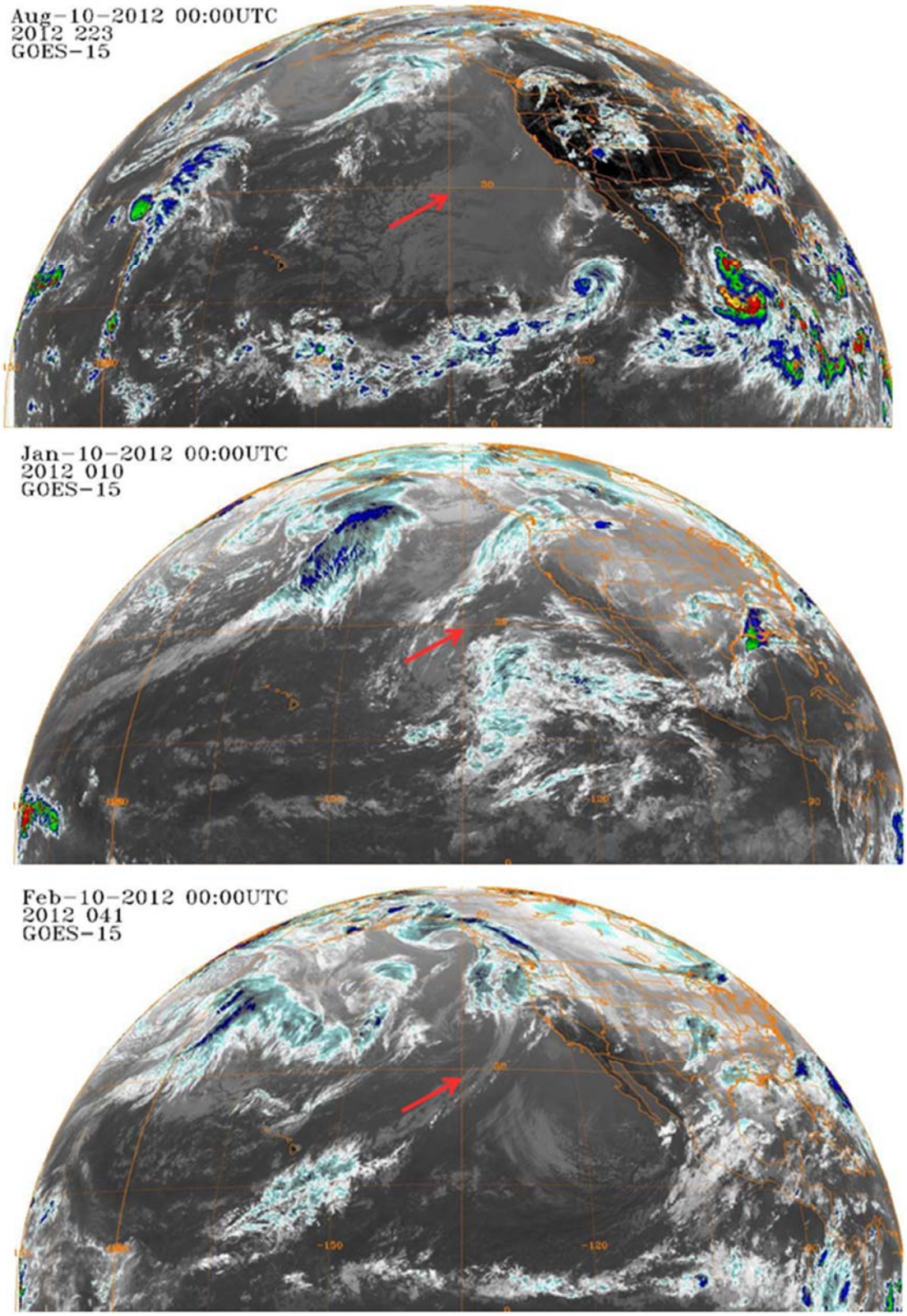


*Figure 9: Near-infrared images from geostationary satellite GOES 15 on 2012-08-10 00UTC (top panel), 2012-01-10, 00UTC (middle panel) and 2012-02-10, 00UTC (bottom panel). The red arrows point to the approximate location (30N, 140W) whose vertical error characteristics are examined in the text. GOES Images from NOAA National Climatic Data Centre.*

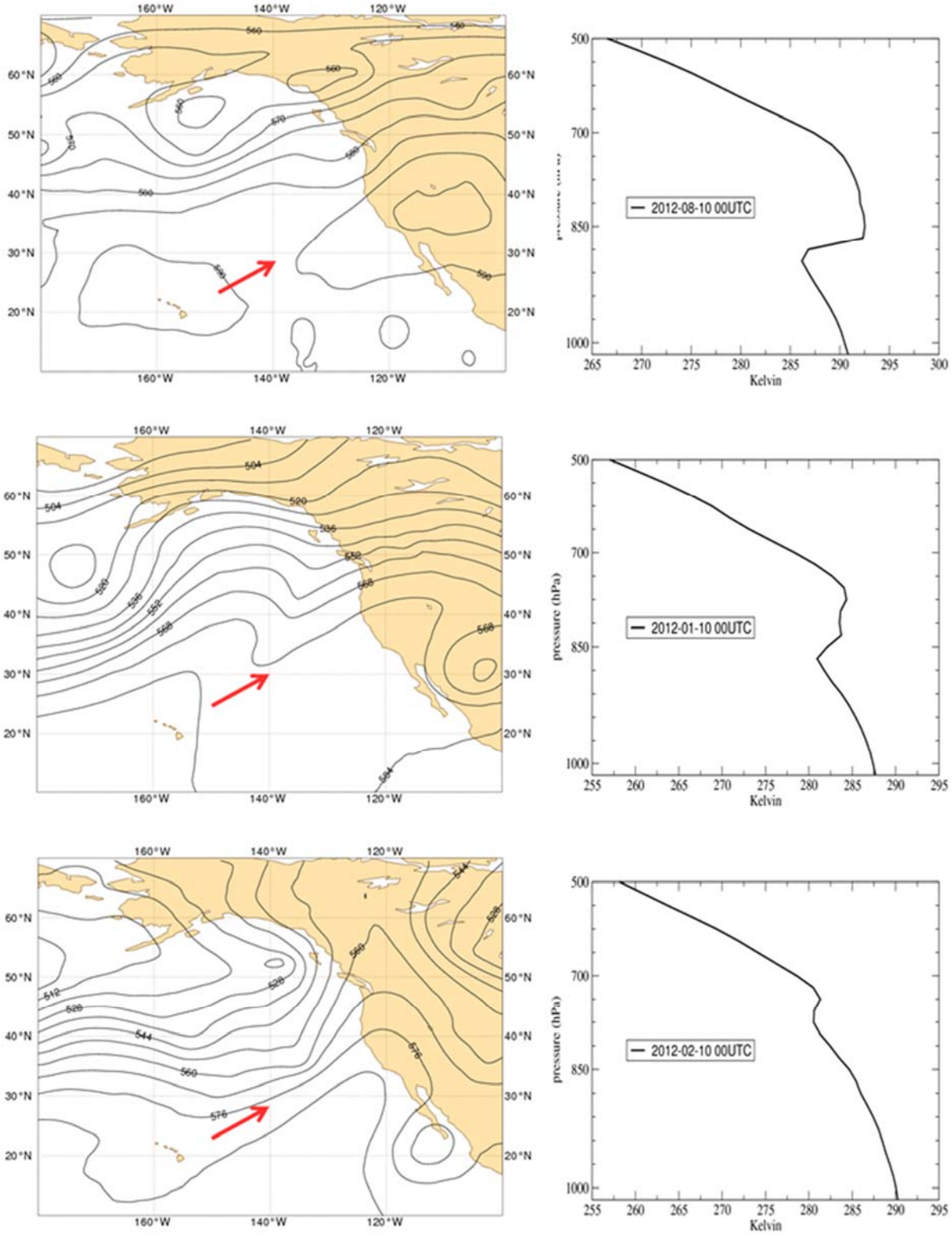


*Figure 10: Analysed 500 hPa geopotential (left column) and vertical profile of temperature in the lower troposphere at (30N, 140W) valid on 2012-08-10 00UTC (top panel), 2012-01-10, 00UTC (middle panel) and 2012-02-10, 00UTC (bottom panel). The red arrows point to the approximate location (30N, 140W) whose vertical error characteristics are examined in the text.*

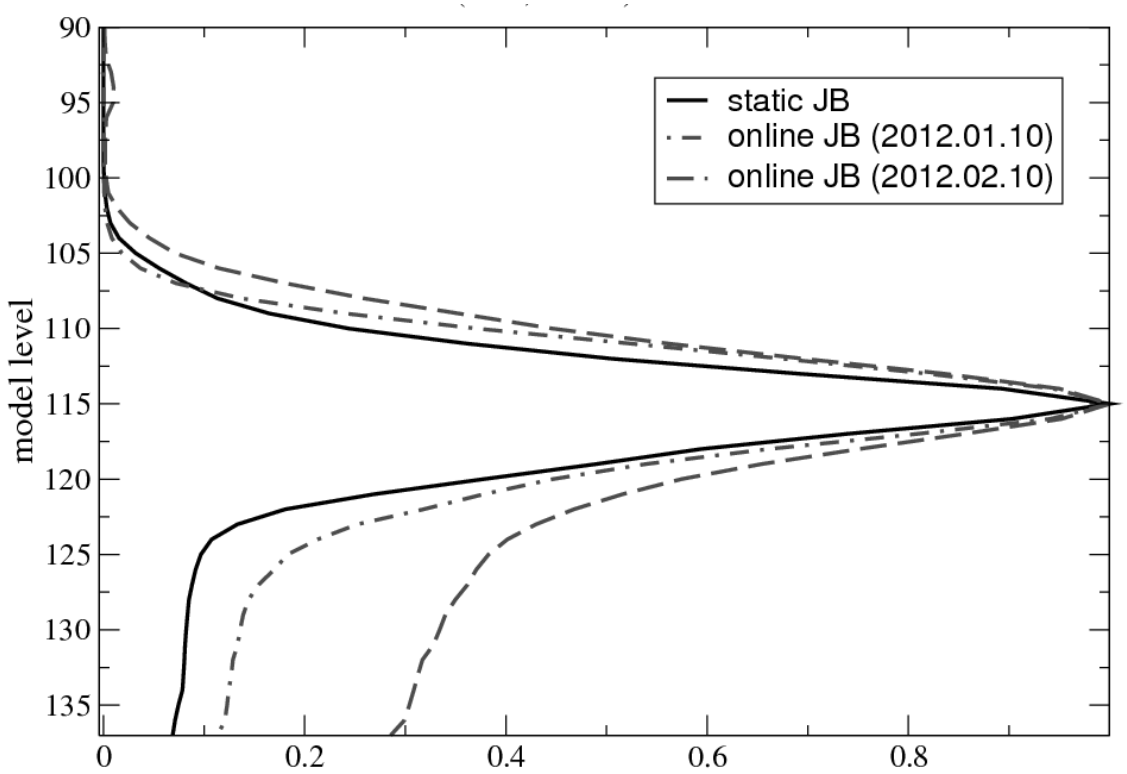


*Figure 11: Vertical correlation of background errors of vorticity at model level 115 (ca. 850 hPa) in the vicinity of (30N, 140W) diagnosed from: the static wavelet* **B** *(continuous line); the online wavelet* **B** *valid on 2012/01/01 at 00UTC (dash-dot line); and the online wavelet* **B** *valid on 2012/02/01 at 00UTC (dashed line). Note that model level 137 is the bottom level of the current IFS model (ca. 10m above the model surface) and model level 90 corresponds approximately to 400 hPa.*

The ability of the online estimates of the wavelet **B** to track the impact of slowly evolving synoptic patterns on the error structure functions also benefits forecast skill. This can be appreciated from Fig. 12 (for the Extra-Tropics) and Fig. 13 (for the Tropics). Skill improvement is seen to be relatively small (in the 0.5% to 1.5% range) but homogeneous and often statistically significant at the 95% level. An interesting feature of these plots is that they tend to show larger improvements with height, possibly because of the typically smoother and slower modes of variability of the error dynamics in the high troposphere and stratosphere, which the spatially and temporally smoothed correlations structures estimated by the online wavelet **B** are better able to represent. These positive results led to the operational implementation of the online wavelet **B** with lagged EDA perturbations at ECMWF in IFS cycle 40R1 (November 2013).

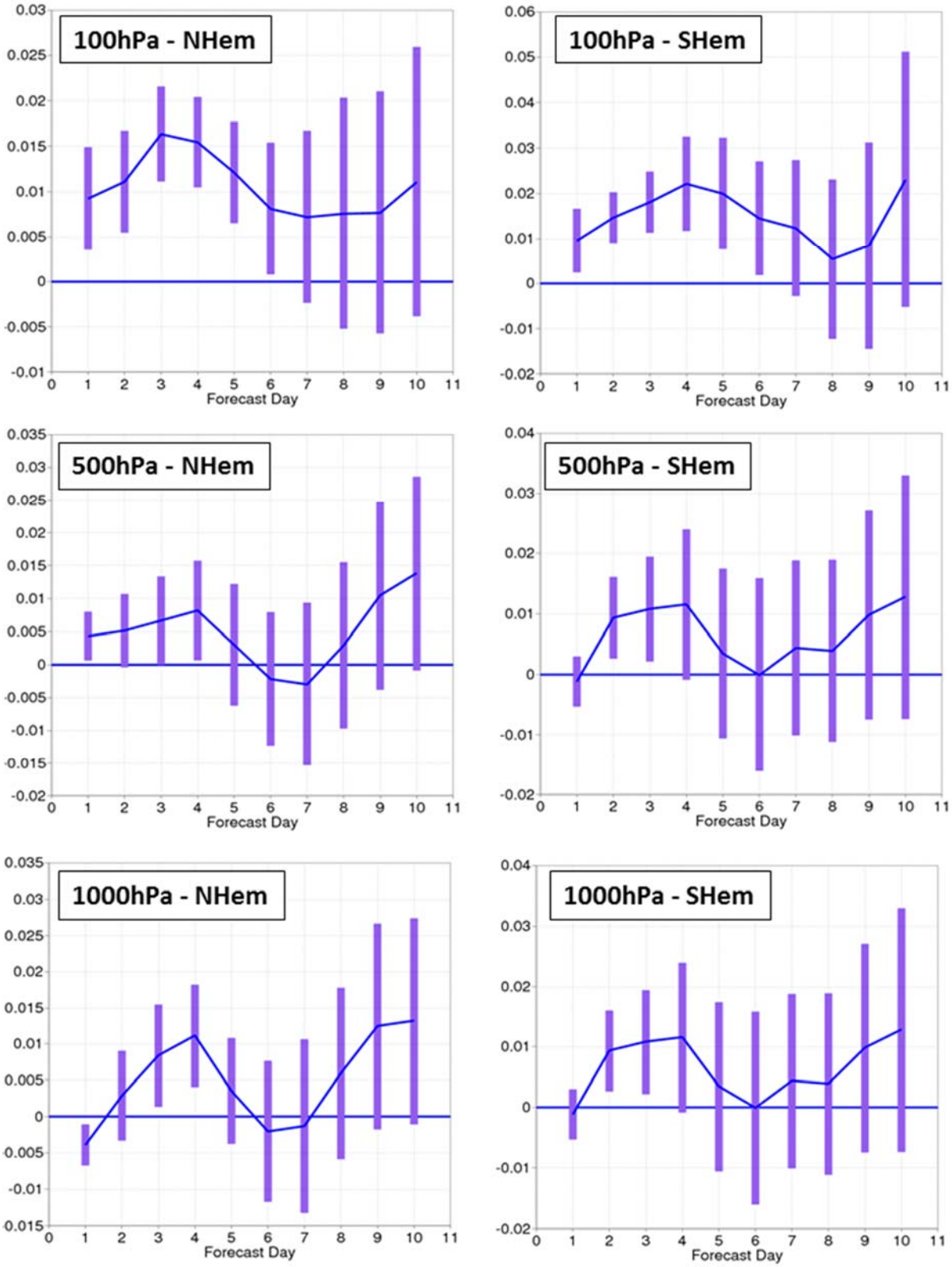


*Figure 12: Normalized difference of root mean square errors of geopotential forecasts from two assimilation cycles using climatological vs. online wavelet* **B** *(positive values indicate smaller errors of online wavelet* **B** *cycle). Left column refers to Northern Hemisphere, right column to Southern Hemisphere. Top row: 100 hPa; middle row: 500 hPa; bottom row: 1000 hPa. Scores are averaged over the period 20120201-20120605 and use the ECMWF operational analysis as verification.*

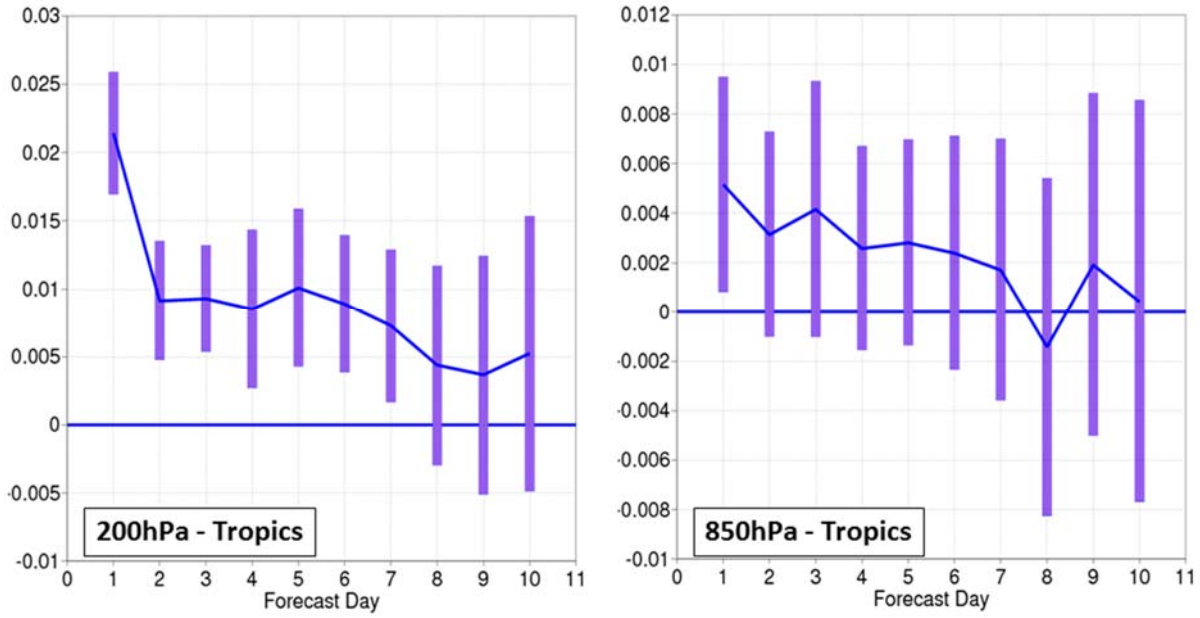


*Figure 13: Normalized difference of root mean square errors of wind vector forecasts from two assimilation cycles using climatological vs. online wavelet* **B** *(positive values indicate smaller errors of online wavelet* **B** *cycle). Scores are computed for the Tropics at 200 hPa (left panel) and 850 hPa (right panel). Scores are averaged over the period 20120201-20120605 and use the ECMWF operational analysis as verification.*

b) Hybrid wavelet **B** estimates.

One deficiency of the online estimation of the wavelet **B** described above is that a systematic phase shift will be introduced in the location of the estimated correlation structures with respect to the relevant atmospheric state. In the operational configuration, with a 25 member EDA and 12 day training period, the estimated wavelet **B** mainly presents variability in the weekly and sub-monthly scales. Reducing the training dataset time window to 3-6 days by increasing number of EDA members will not improve upon this, but result in correlations that neither represents the prevailing flow-regimes nor the more transient errors of the day. This is probably why experiments using lagged perturbations of a 50 member EDA over a 6 day period showed a degradation of scores in the Northern Hemisphere (not shown). For this reason an alternative approach has been explored that combines 200 samples from the latest 25 member EDA (eight hourly time steps centred around the background time) representing the errors of the day, with 400 EDA samples spread throughout the year representing the "climatology" of errors for average weather conditions and observation system coverage. This large training dataset allows avoiding the use of filtering and covariance localization on the sampled **B**.

The hybrid wavelet B uses current EDA perturbations as a flow-dependent modification of average errors to avoid the phase-shift of correlation structures present in the online formulation discussed above. An example is given in Fig. 14 where a snapshot of the background error length scales of vorticity at 100 hPa (top panels) and near the surface (bottom panels) for the online wavelet **B** (left panels) and hybrid wavelet **B** (right panels) is shown. The correlation structures diagnosed by the hybrid wavelet **B** have a closer connection with the current meteorological situation. Note, in particular, how the error correlations diagnosed by the hybrid wavelet **B** near the surface (bottom right panel) reflect the sharp frontal pressure gradients visible in the region.

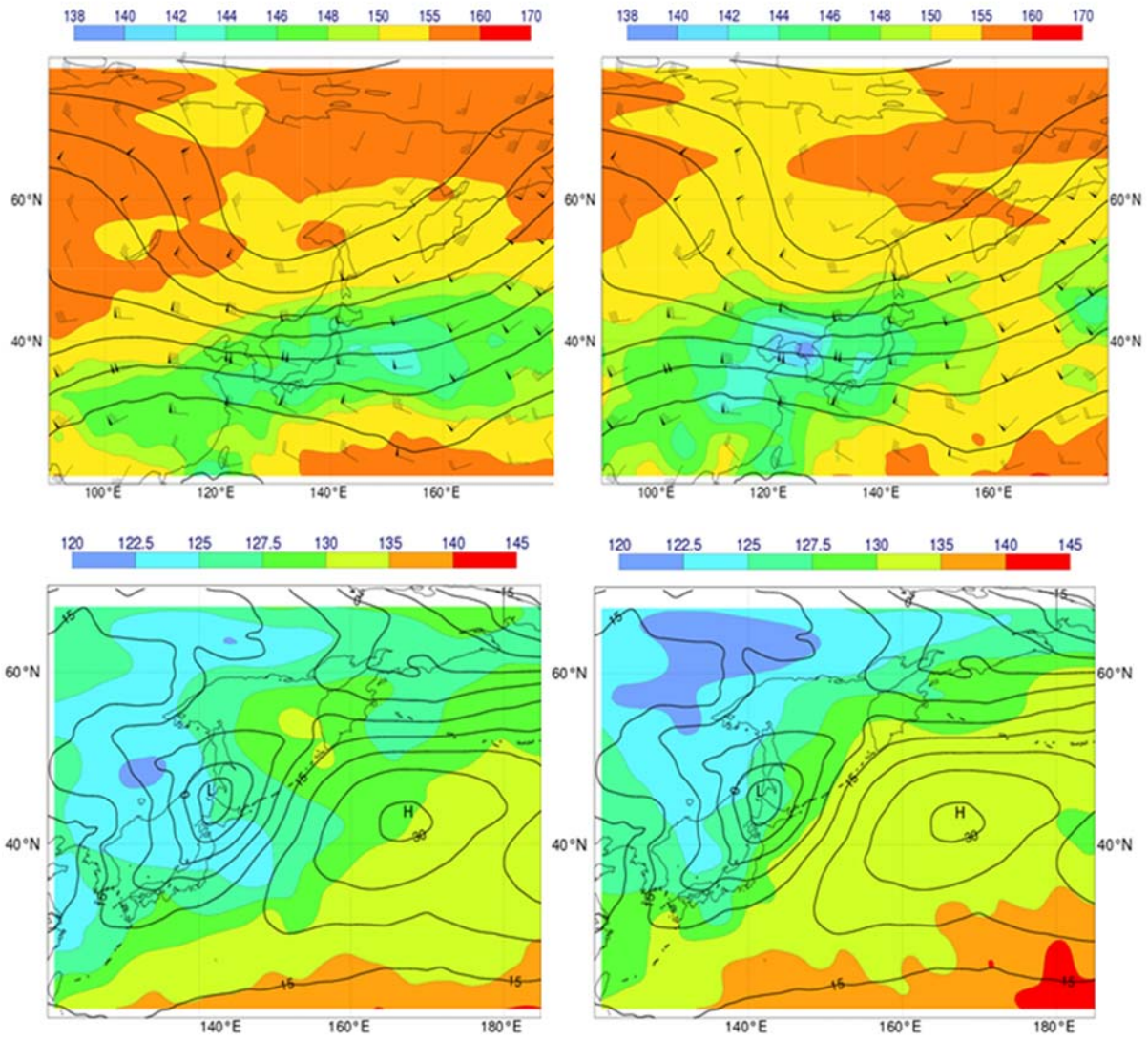


*Figure 14: Background error length scales (shaded; units: km)) for vorticity at model level 60 (ca. 100 hPa; top panels) and model level 137 (surface; bottom panels) diagnosed from the online wavelet B (left panels) and the hybrid wavelet B (right panels), valid on 09/11/2013 at 21UTC. Isolines of background 100 hPa (top panels) and 1000 hPa (bottom panels) geopotential height forecast valid at the same time (solid line, units: $10^2$ $m^2/s^2$) and wind barbs (units: knots) at 100 hPa are superimposed.*

The impact of the hybrid wavelet **B** on the assimilation cycle is small but significantly positive throughout the atmospheric column (Fig. 15). A larger impact is seen on the forecast skill scores (Fig. 16), especially in the lower stratosphere. This impact is visible not only in the RMS forecast error metric, as shown, but also, to a large extent, in the standard deviation and anomaly correlation metrics. This indicates that the improvement in this set of sensitivity experiments does not primarily originate from a change in the mean analysed and forecasted atmospheric state. It is still expected, however, that the introduction of a climatological component in the **B** estimates would prove beneficial for controlling forecast model biases in the assimilation cycle, as these tend to be dependent on the prevailing meteorological situation (e.g., stable boundary layer, stratospheric temperature biases; see also Danforth and Kalnay, 2008, for a discussion in the EnKF context).

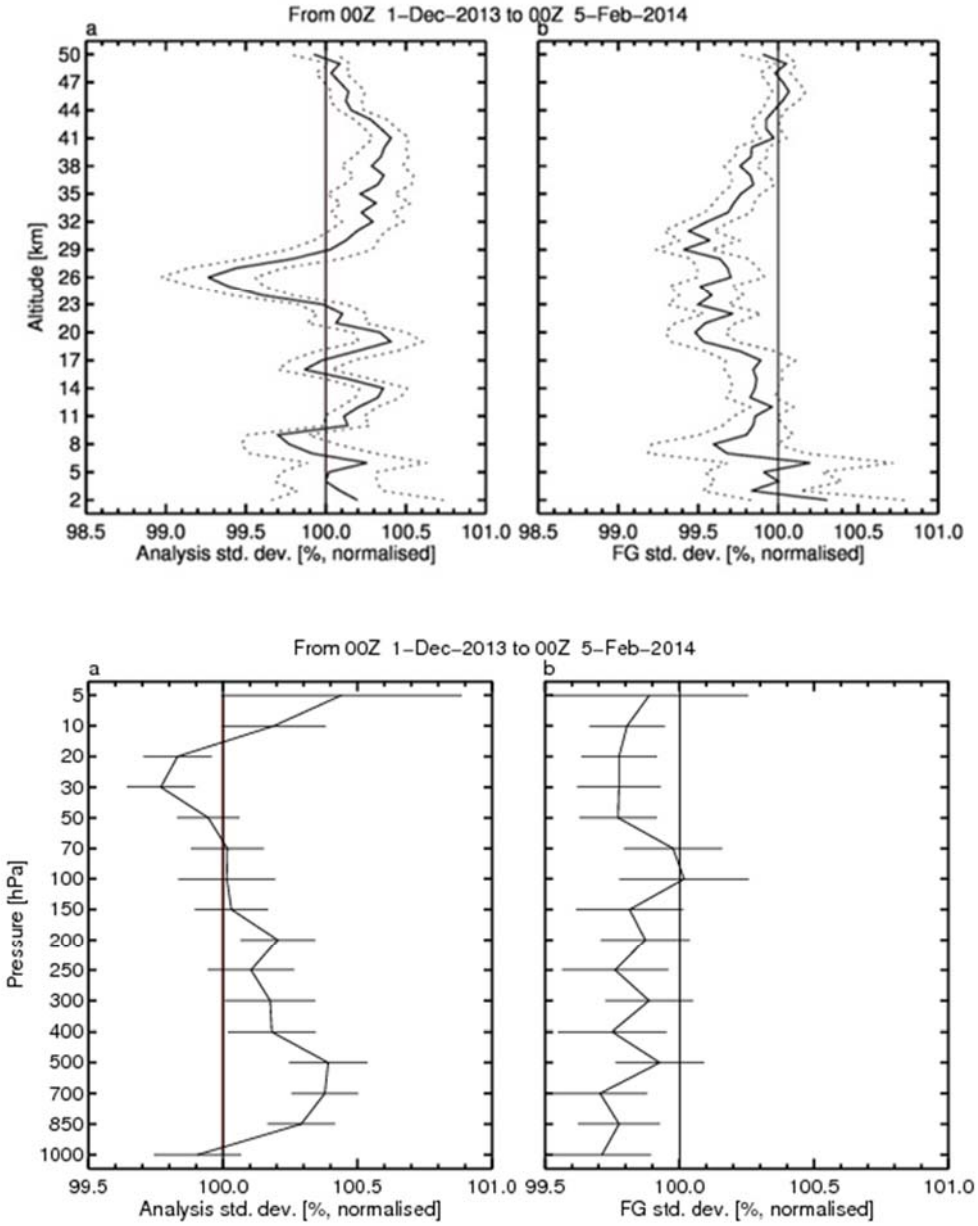


*Figure 15: Normalised change in the standard deviation of analysis departures (left column) and background departures (right column) of assimilated GPSRO observations (top panels) and radiosonde temperature observations (bottom panels) for an experiment using the hybrid wavelet* **B** *with respect to an experiment using the online wavelet* **B**. *Global values averaged over the 1/12/2013 - 5/2/2014 period.*

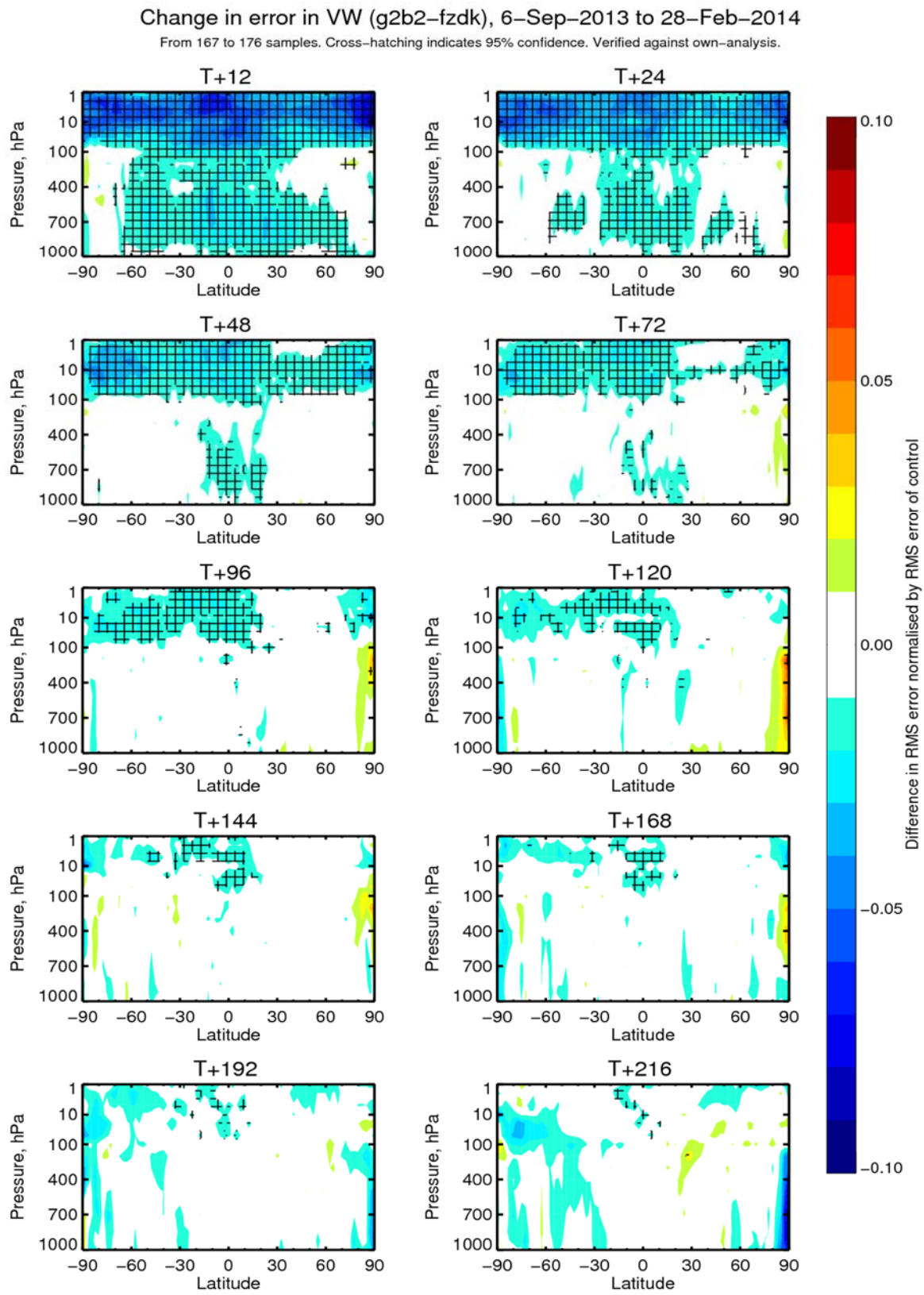


*Figure 16: Normalised change in the RMS wind vector forecast errors for an experiment using the hybrid wavelet B with respect to an experiment using the online wavelet B. Values averaged over the 6/9/2013 - 28/2/2014 period. Verification is against own analysis. Cross hatching indicates 95% confidence level.*

# 4 Impact of EDA resolution on 4DVar error estimates

The EDA (Isaksen et al., 2010) should ideally be run with the same Kalman gain and in particular at the same resolution as the target assimilation cycle whose error covariances need to be simulated. In practice it is not affordable to run an ensemble system such as the EDA at the high resolution of the operational 4DVar assimilation cycle, but narrowing the resolution gap should improve the realism and accuracy of the simulated errors. This is confirmed by Houtekamer et al., 2014, who showed, in a similar context of an EnKF with perturbed observations, how an increase in horizontal resolution of the ensemble was the major driver behind recent improvements in the performance of the EnKF system at Environment Canada.

The current operational setup of the EDA is based on a set of 25 independent 4DVar analysis cycles with perturbed observations, model physics and sea surface temperatures (Isaksen et al., 2010). The incremental 4DVar analysis step is run at an outer loop resolution of TL399 spectral truncation (ca. 50 km grid spacing) and two inner loop minimizations at TL95 and TL159 spectral truncation (ca. 210 and 125 km grid spacing). TL399 is also the resolution at which the nonlinear forecast model is run to cycle the analysis fields. This configuration was chosen based on a detailed investigation of cost and performance characteristics of the EDA (see Isaksen et al., 2010). The HRES 4DVar is currently run at TL1279 outer loop resolution (ca. 15 km grid spacing) with three inner loop minimizations at TL159, TL255, TL255 spectral resolution (ca. 125 and 80 km grid spacing). Here too the resolution of the outer loop trajectories is the same as the forecast model. The vertical resolution is the same for both systems (137 hybrid vertical levels). At these resolutions the EDA computational cost is already large (about 3 times that of the HRES data assimilation system). The most expensive components of the EDA 4DVar analysis are the inner loop minimizations as these require ca. 30 integrations of the tangent linear and adjoint models over the assimilation window. On the other hand, a relatively inexpensive part of the EDA 4DVar setup is the resolution at which the outer loop trajectories and the background forecast model are run, since these require only a few nonlinear model integrations. Increasing the horizontal resolution of the EDA from the current T399 (50 km grid spacing) to T639 (30 km) would have a relatively minor impact on the computational cost of the system. For these reasons a limited study has been conducted by running for a month (August 2013) two EDAs at T399 and T639 outer loop resolutions in order to evaluate the impact of this change on the resulting error estimates.

The increase in horizontal resolution naturally leads to more realistic estimates of the uncertainties of the data assimilation cycle, especially for intense, localised weather systems An example is given in Fig. 17, where the two estimates (from the T399 and the T639 EDAs) of surface pressure background uncertainty during the lifecycle of typhoon Bolaven are contrasted. See also Isaksen et al., 2010, for other examples of the benefit of increased outer loop resolution for the representation of errors associated with tropical cyclones.

In time and globally averaged terms, the increase in resolution produces an increase of around 15% to 25% in the magnitude of the estimated vorticity background errors and a vertically increasing growth of the unbalanced temperature errors between 5% and 20%. To put these numbers into context, it is worth recalling that the current ECMWF EDA perturbations need to be inflated with a global factor of 1.35

(i.e., 35% inflation; Bonavita et al., 2012) in order to produce realistic levels of spread. Figure 18 shows the monthly average latitudinal distribution of the increase in EDA spread. Most of the increase is located in the Extra-Tropics at mid-tropospheric and stratospheric levels. This indicates that the more active dynamics of the T639 model is better able to capture the uncertainties in the evolution of extra-tropical weather systems.

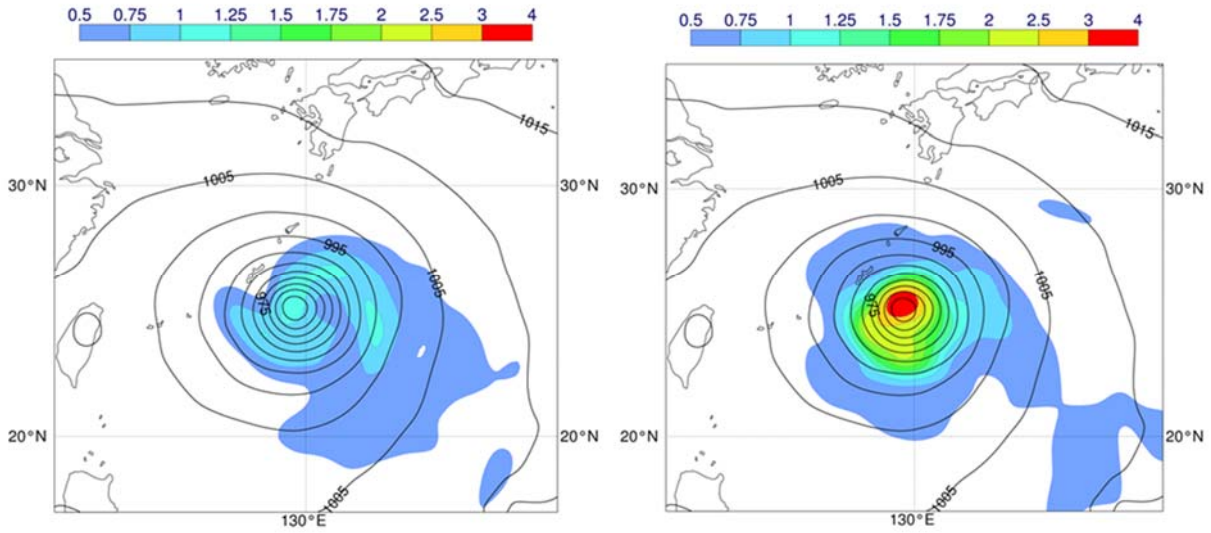


*Figure 17: Background error standard deviations (shaded; units: hPa) for surface pressure diagnosed from a T399 EDA (left panel) and a T639 EDA (right panel), valid on 25/08/2013 at 21UTC, and background mean sea-level pressure forecast valid at the same time (solid line, units: hPa)*

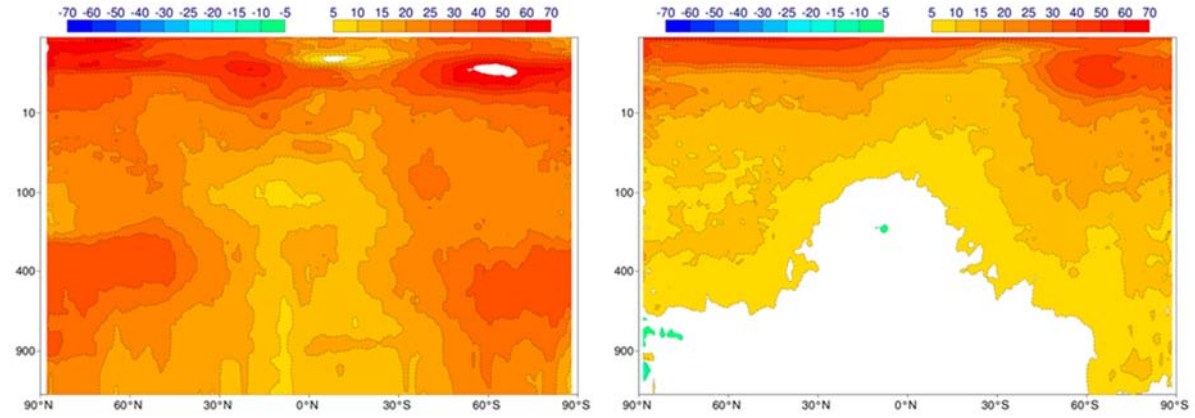


*Figure 18: Vertical profiles of the longitudinally averaged relative change between the T639 EDA and the T399 EDA of EDA standard deviations of vorticity (left panel) and unbalanced temperature (right panel). Values are time averaged over 1 month (August 2013).Units in Kelvin (temperature) and $s^{-1}$ (divergence). Vertical axis in pressure levels (hPa).*

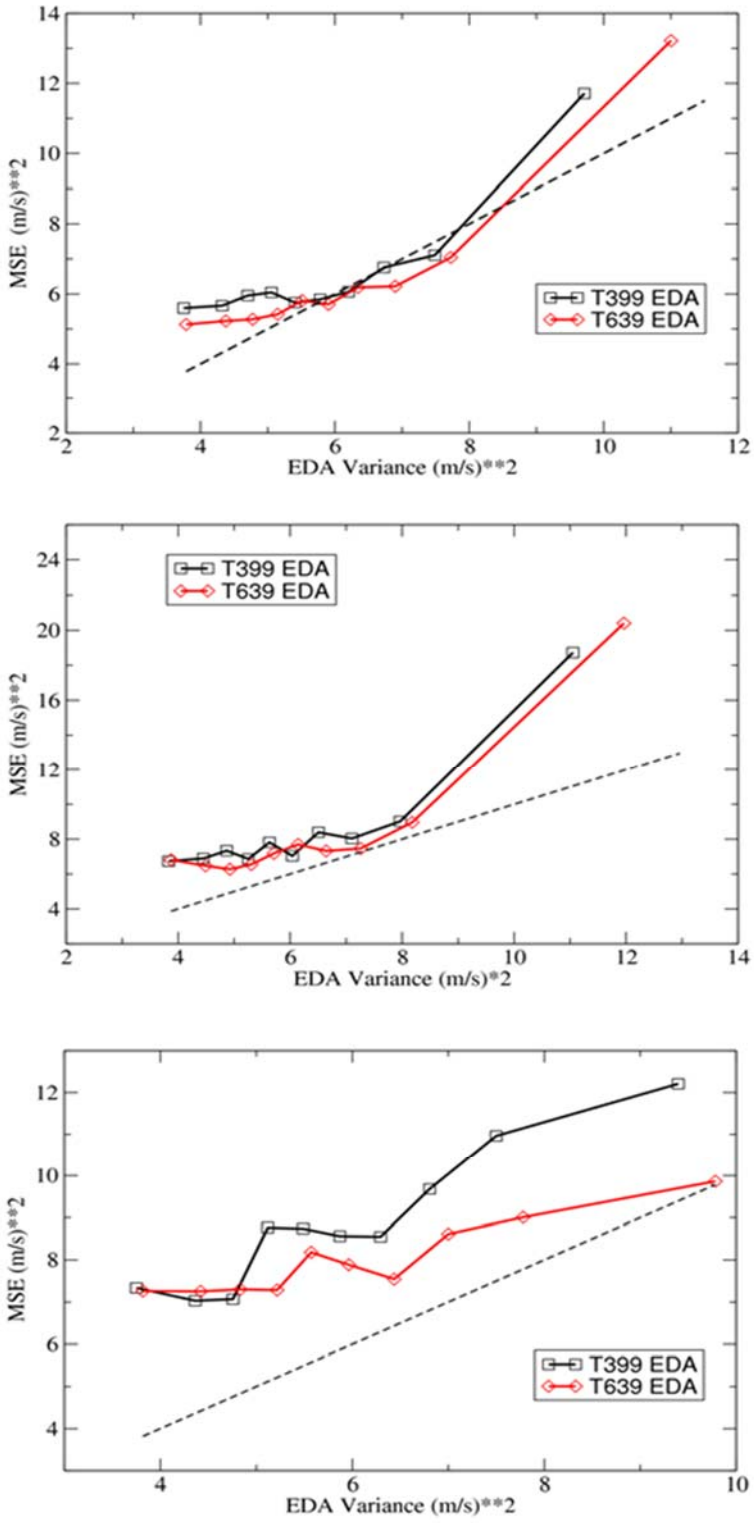


*Figure 19: Spread-Skill curves of the 850 hPa zonal wind in the Northern Hemisphere (top panel), Tropics (middle panel) and Southern Hemisphere for the T399 EDA (black continuous line) and the T639 EDA (red continuous line). See text for further details.*

The statistical properties of the two EDA experiments can also be diagnosed in observation space. In Fig. 20 we present the spread-skill diagnostic curves for 850 hPa zonal wind for the two EDA experiments. These curves are based on the standard reliability condition of the innovation statistics:

$$<(\mathbf{y}-\mathbf{Hx})^2> = \mathbf{HP}^b\mathbf{H}^T + \mathbf{R} \qquad (2)$$

and the result (Isaksen et al., 2010) that for a reliable EDA

$$\mathbf{HP}^b\mathbf{H}^T = \frac{1}{N-1}\sum_{i=1,N}(Hx_i - \overline{Hx})^2 = \mathrm{VAR}_{\mathrm{EDA}} \qquad (3)$$

where $N$ is the number of EDA members. In the plots the y-axis represents the mean squared value of the radiosonde innovations (observation-background) computed for the control (unperturbed) EDA member, while the x-axis represents the EDA background variance at the observation locations. The sample population of variances and innovations has been divided into ten equally populated bins according to their EDA background variance magnitude and the dashed line represents the line where the bin-averaged variance-innovation points should lie for a statistically consistent EDA. Besides the general increase in spread, the T639 EDA is more statistically consistent than its T399 counterpart. The larger relative impact seen in the Southern Hemisphere likely reflects the locally more active weather conditions prevalent during the August period of the experiment.

# 5 Discussion

The use of ensembles to diagnose flow-dependent background error covariances has been one of the main development themes in operational atmospheric data assimilation over the past ten years. The common approach to use ensemble information in pre-existing variational systems has been to make direct use of ensemble perturbations to sample the **B** matrix either at the start of the assimilation window (through augmentation of the control vector: "alpha control variable") or throughout the whole assimilation window (4D-En-Var). The strategy followed at ECMWF to incorporate ensemble information into the operational 4DVar assimilation cycle has been different, with ensemble information gradually incorporated into the **B** model which describes the background error covariance matrix at the start of the assimilation window. These incremental changes have been shown to be beneficial both in terms of improving the realism of the modelled **B**, and, more importantly, in terms of giving measurable improvements in the accuracy of the analysis and forecast fields produced by 4DVar assimilation cycle which made use of the online **B**.

The success of the ECMWF data assimilation strategy has in large part been based on having a realistic error cycling model (EDA), a sophisticated representation of the EDA-based background errors in the 4DVar analysis through the ECMWF wavelet **B** model, and having very accurate tangent linear and adjoint representations for the prognostic model and the observation operators. These set of factors have allowed obtaining a reasonably accurate representation of background errors throughout the assimilation window, while also avoiding the need to apply spatial localization to the sampled covariances. While there are some currently unresolved issues (for example the negative forecast impact that the use of the mass-wind balance constraints produces in the middle and upper stratosphere), the discussion above indicates that the current ECMWF **B** model, trained with an evolving dataset of EDA perturbations, is already able to capture many of the desirable features of ensemble-based sampled **B** covariances and is

a flexible enough framework to allow further refinements along the development lines considered above. It is however conceivable that, as the spatial resolution of the model and the data assimilation system increase, the expected decrease in correlation length scales, their increased anisotropy, the sharper error gradients and the increased flow-dependent aspects of the balance relationships (Ménétrier et al., 2014; Brousseau et al., 2011, 2012) would pose greater challenges to the current **B** model. Whether the further development of the **B** model or a more direct use of ensemble information is the more cost effective solution is an important open research question.

Another central aspect of the ECMWF data assimilation system is the EDA. The EDA is constructed to be a Monte Carlo simulation of the errors of the HRES data assimilation cycle. As such, it is important that the resolution of the EDA be as close as practically possible to that of the target system if EDA perturbations are to be representative of the HRES data assimilation system errors. In fact, it has been shown above that increasing the outer loop resolution of the EDA from T399 to T639, still only half that of the current resolution of the HRES 4DVar, is able to account for a large fraction of the current under-dispersiveness of the EDA-based error estimates. This is significant because this resolution upgrade would significantly reduce the need to use parameterized representations of model error in the EDA. Unfortunately, the EDA is also a computationally expensive system, both because of its stochastic nature and because it is based on a 4DVar solution of the Kalman Filter update equation. For this reason, current research is focussed on improving the efficiency of the EDA as much as possible without compromising its defining characteristics and on evaluating cheaper alternatives for the error cycling of the HRES data assimilation based on a hybrid EnKF system of the type described in Hamrud et al. (2014).

# 6 Summary

At ECMWF flow-dependent ensemble information from EDA has gradually been incorporated into the **B** model which describes the background error covariance matrix at the start of the assimilation window. Starting with background error variances for the balanced part of the control vector and observation quality control (Bonavita et al., 2012) this study extends the flow-dependency to background error variances for the unbalanced part of the control vector and for background error correlation structures. The correlations are determined either online from previous days or from a hybrid of climatological and current cycle background perturbations. About 600 samples are needed for robust correlation estimates for the ECMWF 137 level model, and with 25 ensemble members and 12 hour cycling the online formulation uses samples from previous 12 days whereas the hybrid formulation combines 200 samples from current cycle (8 hourly time steps centred around start of the assimilation window) with 400 samples spread throughout the year. Each of these changes is shown to improve both the realism of the modelled **B** and the accuracy of the analysis and forecast fields produced by the 4D-Var assimilation cycle which makes use of the improved B. The current ECMWF wavelet **B** model, trained with an evolving dataset of EDA perturbations, already captures many features of ensemble-based sampled **B** covariances. However, the anisotropy of background errors and flow-dependency of balance relationships may increase with model resolution. To address this, further developments of the wavelet **B** model and balance operator (e. g. anisotropic correlations through coordinate transforms, see Dee and Gaspari 1996 and Michel 2012) and/or a more direct use of ensemble information will be required

It is also shown that moving the resolution of the EDA closer to the target high resolution data assimilation cycle improves the realism of background error variances. Moving the EDA outer loop and

forecast resolution from T399 to T639 (half of the T1279 high resolution) removes more than half of the current under-dispersiveness of the EDA-based error estimates and reduces the amplitude of the stochastic parameterized model error perturbations needed in the EDA.

# REFERENCES

Barker, D. M. (1999): Var scientific development paper 25: The use of synoptic-dependent error structure in 3DVAR. Met Office Tech. Rep., 2 pp. [Available from Met Office, FitzRoy Rd., Exeter, Devon EX1 3PB, United Kingdom].

Belo Pereira, M. and L. Berre (2006): The use of an ensemble approach to study the background-error covariances in a global NWP model. *Mon. Wea. Rev.*, **134**, 2466–2489.

Berre, L., O. Pannekoucke, G. Desroziers, S. E. Stefanescu, B. Chapnik and L. Raynaud (2007): A variational assimilation ensemble and the spatial filtering of its error covariances: increase of sample size by local spatial averaging. *Proceedings of the ECMWF Workshop on flow-dependent aspects of data assimilation* ECMWF, pages 151-168.
(Available from: http://www.ecmwf.int/publications/)

Bishop, C. H., and D. Hodyss (2011): Adaptive Ensemble Covariance Localization in Ensemble 4D-VAR State Estimation. *Mon. Wea. Rev.*, 139, 1241-1255

Bonavita, M., L. Raynaud and L. Isaksen (2011): Estimating background-error variances with the ECMWF Ensemble of Data Assimilations system: the effect of ensemble size and day-to-day variability. *Q. J. R. Meteorol. Soc.*, **137**: 423–434.

Bonavita M., L. Isaksen and E. Holm (2012): On the use of EDA background error variances in the ECMWF 4D-Var. *Q. J. R. Meteorol. Soc.* 138, 1540-1559.

Bonavita, M. (2014): On some aspects of the impact of GPSRO observations in global numerical weather prediction. *Q.J.R. Meteorol. Soc.* doi: 10.1002/qj.2320

Bouttier, F., J. Derber and M. Fisher (1997): The 1997 revision of the Jb term in 3D/4D Var. *ECMWF Technical Memorandum,* 238. (Available from: http://www.ecmwf.int/publications/)

Brousseau P., Berre L., Bouttier F. and G. Desroziers (2011): Background-error covariances for a convective-scale data-assimilation system: AROME-France 3D-Var. *Q. J. R. Meteorol. Soc.* 137: 409–422.

Brousseau, P., Berre, L., Bouttier, F. and Desroziers, G. (2012): Flow-dependent background-error covariances for a convective-scale data assimilation system. *Q.J.R. Meteorol. Soc.*, 138: 310–322.

Buehner, M. (2005): Ensemble-derived stationary and flow-dependent background error covariances: Evaluation in a quasi-operational NWP setting. *Q. J. R. Meteorol. Soc.*, **131**: 1013–1043.

Buehner, M., P. L. Houtekamer, C. Charette, H. L. Mitchell, and B. He (2010a): Intercomparison of Variational Data Assimilation and the Ensemble Kalman Filter for Global Deterministic NWP. Part I: Description and Single-Observation Experiments. *Mon. Wea. Rev*., 138, 1550-1566.

Buehner, M., P. L. Houtekamer, C. Charette, H. L. Mitchell, and B. He (2010b): Intercomparison of Variational Data Assimilation and the Ensemble Kalman Filter for Global Deterministic NWP. Part II: One-Month Experiments with Real Observations. *Mon. Wea. Rev*., 138, 1567-1586.

Burgers, G., Van Leeuwen, P. J. and Evensen, G. (1998): On the analysis scheme in the ensemble Kalman filter. *Mon. Wea. Rev*. 126, 1719–1724.

Clayton, A. M., Lorenc, A. C. and Barker, D. M. (2013). Operational implementation of a hybrid ensemble/4D-Var global data assimilation system at the Met Office. *Q.J.R. Meteorol. Soc*., 139: 1445–1461.

Danforth, C. M., and E. Kalnay (2008). Using singular value decomposition to parameterize state-dependent model errors. *J. Atmos. Sci*.,65,1467–1478Dee, D.P. and G. Gaspari (1996): Development of anisotropic correlation models for atmospheric data assimilation. Preprint volume, 11th Conf. on Numerical Weather Prediction, August 19-23, 1996, Norfolk, VA, pp. 249-251

Derber J, Bouttier F. (1999): A reformulation of the background error covariance in the ECMWF global data assimilation system. *Tellus* 51A: 195–221.

Evensen, G. (1994). Sequential data assimilation with a nonlinear quasi-geostrophic model using Monte Carlo methods to forecast error statistics. J. Geophys. Res. 99(C5), 10143–10162.

Fisher, M. (2003): Background error covariance modelling. *Proceedings of the ECMWF Seminar on recent developments in data assimilation for atmosphere and ocean*, ECMWF, pages 45–63.
(Available from: http://www.ecmwf.int/publications/)

Hamill, T. M., and C. Snyder (2000): A hybrid ensemble Kalman filter–3D variational analysis scheme. *Mon. Wea. Rev*., 128, 2905–2919.

Hamrud, M., M. Bonavita and L. Isaksen (2014): EnKF and Hybrid Gain Data Assimilation. *ECMWF Technical Memorandum* 733.
(Available from: http://www.ecmwf.int/publications/)

Houtekamer, P. L., Xingxiu Deng, Herschel L. Mitchell, Seung-Jong Baek, Normand Gagnon (2014): Higher Resolution in an Operational Ensemble Kalman Filter. *Mon. Wea. Rev.*, 142, 1143–1162.

Isaksen, L., M. Bonavita, R. Buizza, M. Fisher, J. Haseler, M. Leutbecher and Laure Raynaud (2010): Ensemble of data assimilations at ECMWF. *ECMWF Technical Memorandum* 636.
(Available from: http://www.ecmwf.int/publications/)

Haseler, J. (2004): Early-delivery suite. *ECMWF Technical Memorandum*, 454.
(Available from: http://www.ecmwf.int/publications/)

Hólm, E., E. Andersson, A. Beljaars, P. Lopez, J-F. Mahfouf, A. Simmons and J-N. Thepaut (2002): Assimilation and Modelling of the Hydrological Cycle: ECMWF's Status and Plans. *ECMWF Technical Memorandum*, 383. (Available from: http://www.ecmwf.int/publications/)

Lorenc, A. C. (2003): The potential of the ensemble Kalman filter for NWP—A comparison with 4D-VAR. *Q. J. R. Meteorol.Soc.*, **129**: 3183–3203.

Ménétrier, B., Montmerle, T., Berre, L. and Michel, Y. (2014): Estimation and diagnosis of heterogeneous flow-dependent background-error covariances at the convective scale using either large or small ensembles. *Q.J.R. Meteorol. Soc*., 140: 2050–2061. doi: 10.1002/qj.2267

Michel, Y. (2013): Estimating deformations of random processes for correlation modelling: methodology and the one-dimensional case. *Q.J.R. Meteorol*. Soc., 139: 771–783.

Pannekoucke, O., Berre, L. and Desroziers, G. (2007): Filtering properties of wavelets for local background-error correlations. *Q.J.R. Meteorol. Soc*., 133: 363–379.

Pannekoucke, O., Berre, L. and Desroziers, G. (2008): Background-error correlation length-scale estimates and their sampling statistics. *Q.J.R. Meteorol. Soc*., 134: 497–508.

Pannekoucke, O., Raynaud, L. and Farge, M. (2014): A wavelet-based filtering of ensemble background-error variances. *Q.J.R. Meteorol. Soc*., 140: 316–327.

Raynaud, L., L. Berre, and G. Desroziers (2008): Spatial averaging of ensemble-based background-error variances. *Q. J. R. Meteorol.Soc*., **134**, 1003–1014.

Raynaud, L., L. Berre, and G. Desroziers (2009): Objective filtering of ensemble-based background-error variances. *Q. J. R. Meteorol.Soc*., **135**, 1177–1199.

Raynaud, L., L. Berre, and G. Desroziers (2011): An extended specification of flow-dependent background-error variances in the Météo-France global 4D-Var system. *Q. J. R. Meteorol. Soc.* **137**, 607–619.

Raynaud, L. and Pannekoucke, O. (2012), Heterogeneous filtering of ensemble-based background-error variances. *Q.J.R. Meteorol. Soc*., 138: 1589–1598.

Varella, H., Berre, L. and Desroziers, G. (2011), Diagnostic and impact studies of a wavelet formulation of background-error correlations in a global model. *Q.J.R. Meteorol. Soc*., 137: 1369–1379

Wang X., D. D. Parrish, D. Kleist and J. S. Whitaker (November 2013): GSI 3DVar-Based Ensemble–Variational Hybrid Data Assimilation for NCEP Global Forecast System: Single-Resolution Experiments. *Mon. Weather Rev.*, 141 (11), 4098-4117.